

SUPPORTING INFORMATION for

Vibrational Density of States of Strongly H-Bonded Interfacial Water: Insights from Inelastic Neutron Scattering and Theory

Hsiu-Wen Wang,^{†,1} Mark J. DelloStritto,[‡] Nitin Kumar,^{‡,2} Alexander I. Kolesnikov,[§] Paul R. C. Kent,^{||} James D. Kubicki,[⊥] David J. Wesolowski,[†] and Jorge O. Sofo^{‡,*}

[†]Chemical Sciences Division, [§]Chemical and Engineering Materials Division, ^{||}Center for Nanophase Materials Sciences and Computer Science and Mathematics Division, Oak Ridge National Laboratory, Oak Ridge, Tennessee 37831, United States

[‡]Department of Physics and Materials Research, [⊥]Department of Geosciences Institute, The Pennsylvania State University, University Park, Pennsylvania 16802, United States

*Correspondence to: sofo@psu.edu

¹Current address: Lujan Neutron Scattering Center, Los Alamos National Laboratory, Los Alamos, New Mexico 87545, United States

²Current address: Walter E. Lay Automotive Lab, University of Michigan, Ann Arbor, Michigan 48109, United States

1. SI Fig. S1: The original (unscaled) INS spectra for SnO₂ nanoparticles at two hydration levels (*full* and *dry*), and their comparisons with micron-sized SnO₂ bulk crystallites and ice-Ih spectra

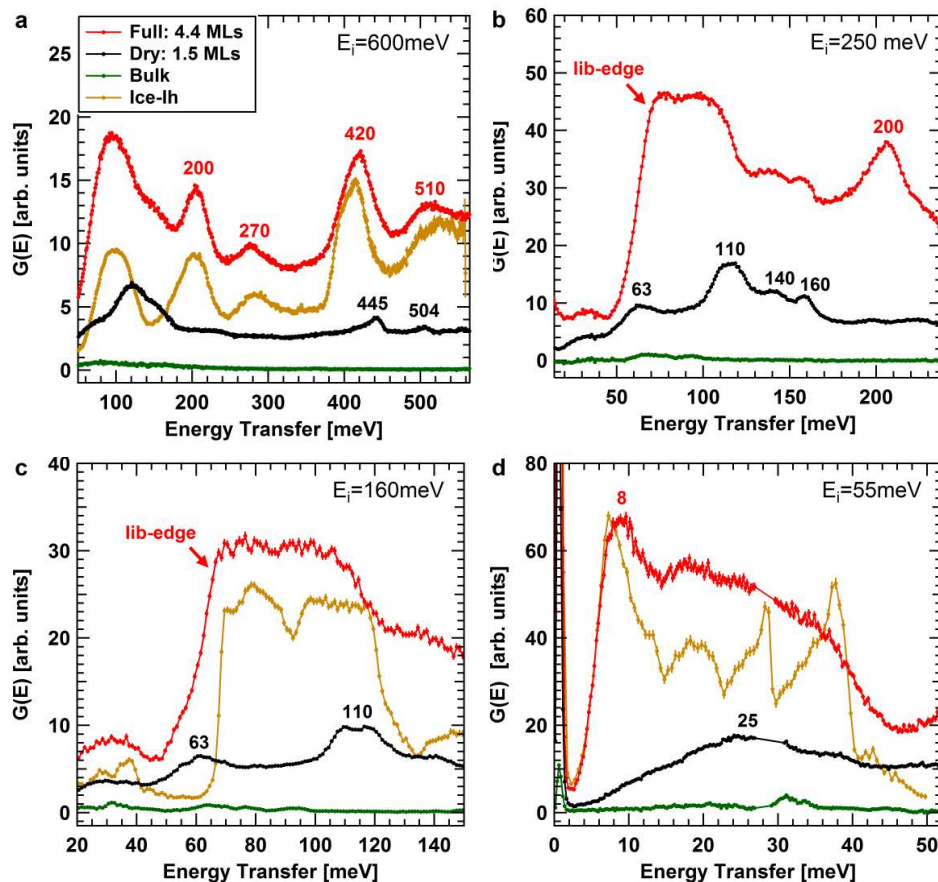


Fig. S1. The INS spectra of the *full* and *dry* nanopowders and micron-sized SnO₂ bulk crystallites, taken with incident neutron energy E_i of (a) 600, (b) 250, (c) 160, and (d) 55 meV at 7K, SEQUOIA (2) beamline. The intensity of VDOS $G(E)$ presented here was only normalized by the weight of each sample, and hence, the decrease of overall $G(E)$ intensity reflects a general decrease in the number of sorbed H₂O/OH species on given surfaces. Accordingly, the minimum surface area corresponds to the bulk SnO₂ sample. The $G(E)$ signal of ice-Ih (plotted for comparison) was normalized using the same area as for the *full* sample under the O-H stretching mode (420 meV; peak fitted with a Gaussian). Errors for each data point are smaller than the symbols.

2. SI Text: Simulation Methods

AIMD: initial preparations and simulations

Although DFT based AIMD simulations were applied to obtain the vibrational spectrum of sorbed water on SnO₂ (110) surface, the relaxation times of water systems are longer than what can be realistically achieved using a DFT-MD approach (3). Therefore, the initial configurations for the DFT-MD simulations were prepared with a classical MD method. A hydrated Sn₂O₄ (110) unit surface was initially generated via placing appropriate number of H₂O molecules above uncoordinated Sn_v sites, and then replicated eight times to achieve the simulated supercell. Four and one H₂O molecules per Sn₂O₄ (110) unit surface were initially prepared for the *full* and *dry* sample cells, respectively. The different dissociation levels (0, 25, 50, 75, and 100%) were conFig.d by transferring one of the H₂O protons (located in L₁ as the innermost layer) to the adjacent BO sites. These initial configurations at a given dissociation level were then relaxed and thermalized at 300K using the force field described in ref. (4) for at least 0.5 ns. Simulations were stopped when the energy drift was negligible.

DFT-MD simulations were performed using the Vienna ab-initio simulation package (5–8). The core electrons were treated with a frozen core projector augmented wave scheme (9, 10). For Sn atoms, the 4d electrons were treated as core, as they are at a low energy far from the Fermi level and thus do not significantly affect the valence states (3). The exchange and correlation potential was treated in the generalized gradient approximation, in accordance to (11, 12).

Calculation of the VDOS G(E) from AIMD

The vibrational spectrum of the SnO₂-H₂O system simulated with AIMD was calculated using the program nMoldyn (v. 3.0.10) (13, 14). nMoldyn is a post-processing program, written by the Theoretical Biophysics, Molecular Simulation, and Scientific Computing Research Group of the National Center of Scientific Research in France, and is specifically designed for the calculation/decomposition of neutron scattering spectra from MD simulations. To obtain the vibrational spectrum of a given MD simulation, nMoldyn calculates the power spectrum of the velocity auto-correlation function (VACF). The VACF of the particles is calculated from the numerical differentiation of the particle positions, the discrete Fourier transform of the VACF can then be applied (15). The VDOS is smoothed by applying a Gaussian window in the time domain, the standard deviation of which is chosen in a manner that all distinct experimental

peaks can be resolved in the calculated spectrum while still retaining a reasonably smooth curve. The greatest advantage of this post-processing calculation is that it allows modification of the trajectories of the atoms in the simulation without significantly altering the accuracy of the calculations. Since the atom trajectories are already set in the trajectory files, any modification of the trajectories for a subset of atoms will affect the vibrational spectrum of that specific subset only. This advantage manifests itself in three useful techniques to decompose the vibrational spectrum of the system: (a) finding the VDOS for a given subset of atoms only, (b) projecting the velocities along given directions, thereby finding anisotropies in the VDOS, and (c) freezing a subset of atoms under certain conditions, thereby eliminating or highlighting difficult to resolve or buried vibrational modes.

To find the VDOS for a given subset of atoms, the sum over power spectrums for only a given subset of atoms is performed. The VDOS along chosen directions can be achieved by multiplying particle positions by a unit vector in those directions and calculating the VACF for the modified trajectories. In this study, we calculated the VDOS along the principal directions parallel with x -, y -, and z -axes (described below), i.e., set all coordinates except those parallel with the given axis to zero. Additionally, when ‘freezing’ atoms in place, we first define a set of geometric conditions that must be satisfied for the atom to be ‘frozen.’ Once the freezing conditions are met in the trajectory file, the atom position is set to be equal to its position at the previous timestep (i.e., forced zero velocity). The atom position is then held at this constant value until the conditions are no longer met. In such a way, the contributions to the VDOS from given configurations can be eliminated while the total number of timesteps of the simulation are still used, which allows one to view the contribution to the VDOS of very short lived configurations ($\leq 10\%$ of the timesteps) with a minimum of numerical noise. The only drawback is that the introduction of a large number of step functions in the velocity can introduce a relatively uniform, low-amplitude noise in the Fourier transform, which drops to zero at high frequencies. However, this noise is nearly constant in the frequency domain of interest, and is not large enough to cover up interesting peaks in the spectrum.

Spectral decomposition and mode assignments on the simulated *dry* sample VDOS $G(E)$

The method described above for the decomposition of the simulated VDOS $G(E)$ is essential for understanding the origin of many features observed in the *dry* sample INS spectra,

including the origin of the 25, 63, 110, 140 and 160 meV peaks and the broad 230-430 meV band resolved from simulation. For clarity, the hydrogen atoms covalently bonded to BO are referred to as ‘trapped-H’, because these hydrogen atoms spend 90% of the simulation time as parts of the BH groups and are constantly trapped between bridging and terminal oxygen (BO and TO) sites via very strong H-bonds (see Fig. 2; main text). In contrast, the hydrogen atoms covalently bonded to TO are referred to as ‘free-H’, because these hydrogen atoms spend roughly 90% of the simulation time as parts of the TH groups and 70% of the time pointing into the vacuum space as free hydroxyl oscillators (see Fig. 2; main text). These free-Hs (in TH groups) can also form weak H-bonds to neighboring TH species 30% of the time. To determine which of the distinct hydrogen atoms (trapped- or free-H) contribute to the simulated/observed spectra in the *dry* sample, the VDOS was calculated for only the free-Hs (in TH groups) and the resulting decomposed spectrum yielded mostly the 25, 63, 110 and 460 meV peaks (Fig. S2; green line), suggesting that the TH group motions in the TH-BH configuration are the main source of these peaks. When the motions of trapped-Hs (in BH groups) were observed in the TH-BH configuration instead, the decomposed spectrum contained the weak 33 and 56 meV peaks, the 140 and 160 meV peaks and the broad 230-430 meV band. Hence, the BH group motions in the TH-BH configuration are the main source of the 140 and 160 meV peaks and the 230-430 meV band (Fig. S2; orange line). By comparison with the spectrum of ice-Ih or ab-initio studies of isolated water molecules for the H₂O librational and intramolecular vibrational modes, it can be readily concluded that the 63, 110 and 460 meV peaks are caused by the wagging (63 and 110 meV) and stretching (460 meV) modes of the TH species in the TH-BH configuration. Similarly, it can be assumed that the 140 and 160 meV peaks correspond to the wagging modes of the BH species and that the 230-430 meV band is due to the stretching modes of the same species in the TH-BH configuration. In addition, since the TW-BO configurations are formed during 10% of the simulation time (due to trapped-H jumping back and forth from a TH-BH to a TW-BO configuration), the corresponding spectrum attributed to such configuration is also computed and illustrated in Fig. S2 (blue line) for the trapped-Hs in the TW configuration only. The small 200 meV peak observed in the INS experiments and resolved from the simulations is mainly related to the TW-BO configuration as a TW H-O-H bending mode.

A dome-like feature centered at about 25 meV is mainly contributed by the TH groups. This 25 meV band is a characteristic of hydroxyl groups tightly bound to the surface with the absence

of a strong H-bond network, as is observed for the *dry* sample surface. Note that SnO₂ lattice modes at about 31 meV are also exhibited (Fig. S1d). Our simulations indicate that the high-energy shoulder of the 25 meV band actually originates from the VDOS of the BOs, which give rise to a feature identical to the orange line shown in Fig. S2 between 0 and 85 meV. This is due to the fact that the motions of trapped-Hs (in BH groups) near these energies are significantly coupled with the BO vibrations via covalent bonds, resulting in modes correlated to the vibrations of BOs.

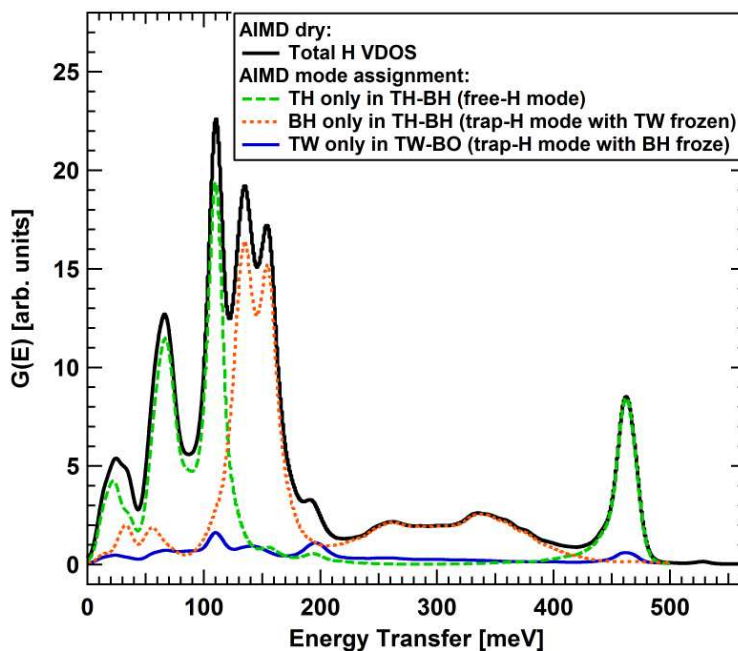


Fig. S2. Hydrogen VDOS from AIMD simulations at 300 K as a function of energy transfer for the *dry* sample. The three decomposed spectra (green, orange and blue lines) show distinct contributions from each subset of hydroxyl and water configurations present on the SnO₂ (110) surface. Note that the broad 230-430 meV band results almost entirely from the stretching of the BH species in the TH-BH configuration.

Further investigations suggest that if a spectrum of trapped-Hs (in BH groups) is projected along a pre-defined vector direction (x -, y -, and z -axes), the resulting spectrum projected in the three orthogonal axes showed the most interesting features. The x -axis is defined as parallel with the lines of the TH/BH rows characteristic for the (110) surface morphology (Fig. 2; main text), the y -axis is defined parallel with the (110) surface and perpendicular to the TH/BH rows, and the z -axis is defined as normal to the (110) surface (Fig. 2; main text). As shown in Figs S3a and S3b, the 140 meV peak almost entirely results from the BH wagging motions along the z -direction, and the 160 meV peak results from the BH wagging motions along the x -direction. These wagging motions normal and parallel to the (110) surface (140 and 160 meV,

respectively) are due to the localization imposed by the surface geometry and the strong H-bond interaction at the surface. This observation is also consistent with the presence of a broad 230-430 meV band when projecting the BH motions along the y -axis. The 230-430 meV band results from an O-H stretching mode corresponding to the formation of strong H-bonds between the TO and trapped-H in the y -direction (Fig. S3c). Note that there is a small contribution to the 140 meV peak from the y -direction and to the 230-430 meV band from the z -direction (Fig. S3). This is due to the fact that the x -, y -, and z -axes are not exactly parallel with the polarization vectors of the system.

Analogous analyses can be applied to free-Hs (in TH groups) for their anisotropic wagging motions and preferential H-bonding directions. Fig. S4 showed the resulting spectrum projected in the same x -, y -, and z - axes as to those shown in Fig. S3. It is clear from Fig. S4 that the 110 meV peak results from the TH wagging motions along both the z - and y -directions (i.e., along the planes perpendicular to the (110) surface), with a very small contribution from the x -direction. The projected motions in the x -axis (Fig. S4b) further suggest that the orientation of TH species is preferentially aligned along the x -direction regardless whether they form weak H-bonds to neighboring TH species or not. The 63 meV peak, on the other hand, mainly results from the TH wagging motions along the x - and y -directions (i.e., along the planes parallel with the (110) surface), with small contributions from the z -direction (Fig. S4). In general, the appearance of anisotropic wagging motions (e.g., 63 and 110 meV in TH groups, and 140 and 160 meV in BH groups) is due mainly to the surface geometry despite of the strength of the surface H-bonds.

More insights into the source/formation of the 230-430 meV band can be gleaned from the pair distribution functions, $g(r)$, of the BO-trapped-H and TO-trapped-H bonding pairs (Fig. S5). Fig. S5a showed the BO-trapped-H $g(r)$ in the covalent (about 1.06 Å) and hydrogen-bond (1.25-2.3 Å) length regions. Since the trapped-H is almost always covalently bonded to a BO (90% of the time), they tend to move as a unit (as correlated atomic motions), which is indicated by the shared peak at about 1.06 Å in the TH-BH configuration (Fig. S5a). This also gives further evidence that the trapped-H contribution to the 25 meV band is coupled with the vibrations of BOs. Correspondingly, the TO-trapped-H bonding pairs in the TH-BH configuration (Fig. S5b) show large hydrogen-bond length variations due to the free movements of the TO atom (which is not a part of the SnO₂ substrate structure). These changes in the H-bond lengths can introduce

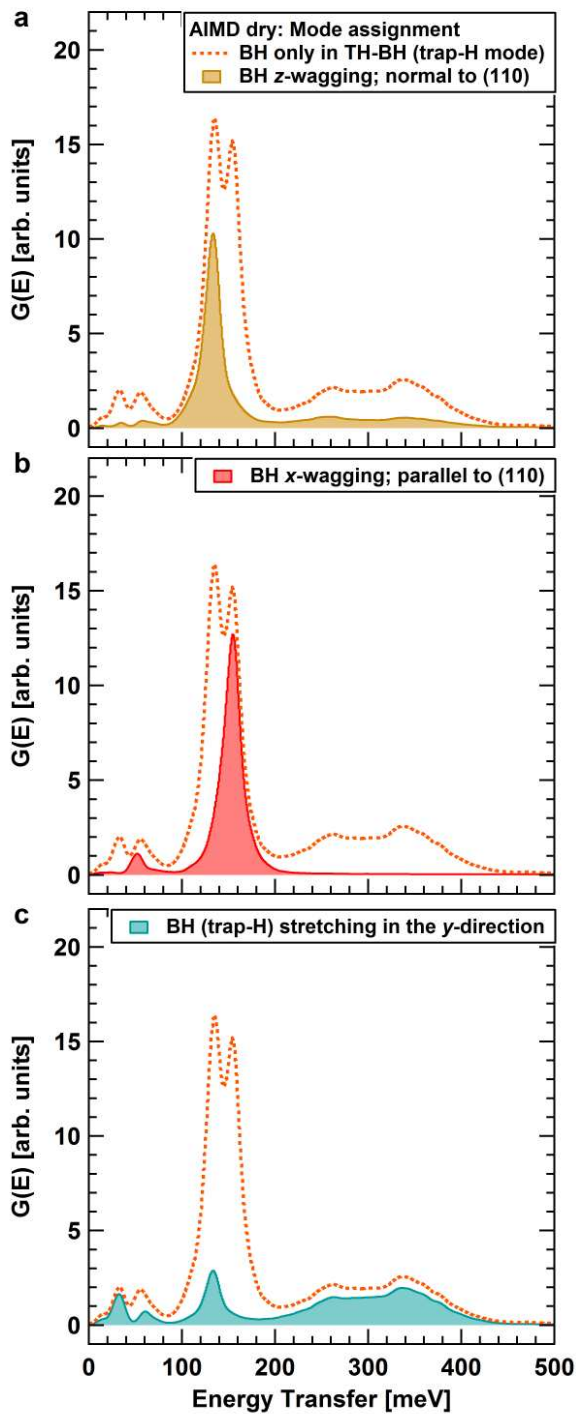


Fig. S3. The AIMD-derived VDOS of the BH species in the TH-BH configuration. The (a) z -, (b) x - and (c) y -projections of the spectrum illustrate the asymmetric BH wagging and stretching motions. Plot (c) suggests that the O-H stretching (230-430 meV) of the BH species is caused by the motion of the trapped-H moving along the lines between the BO and TO sites (the y -direction).

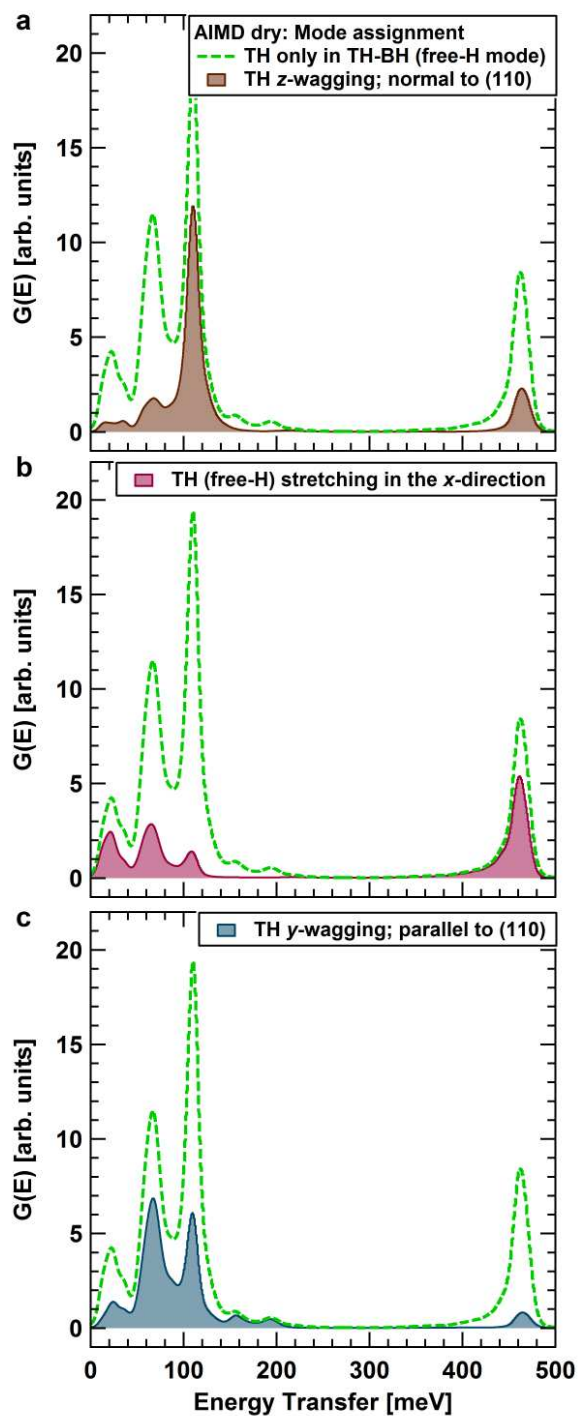


Fig. S4. The AIMD-derived VDOS of the TH species in the TH-BH configuration. The (a) z -, (b) x - and (c) y -projections of the spectrum illustrate the asymmetric TH wagging and stretching motions. Plot (b) suggests that the O-H stretching (460 meV) of the TH species is preferentially aligned along the x -direction.

variable redshifts in the BH stretching mode, as is observed for the broad 230-430 meV band. There is also a possibility that the 230-430 meV band is composed of two low-intensity/broad stretching peaks, one of which is due to BH species (in the TH-BH configuration as discussed above) and the other to TW motions (in the TW-BO configuration). Fig. S2, however, shows that the TW-BO configuration only gives rise to the 200 meV peak resolved in both the simulations (blue line) and in the INS experiments. Thus, the 230-430 meV band corresponds to the stretching mode of the BH species, which is constantly redshifted to various degrees due to the changes in the hydrogen-bond distances between TO and trapped-H.

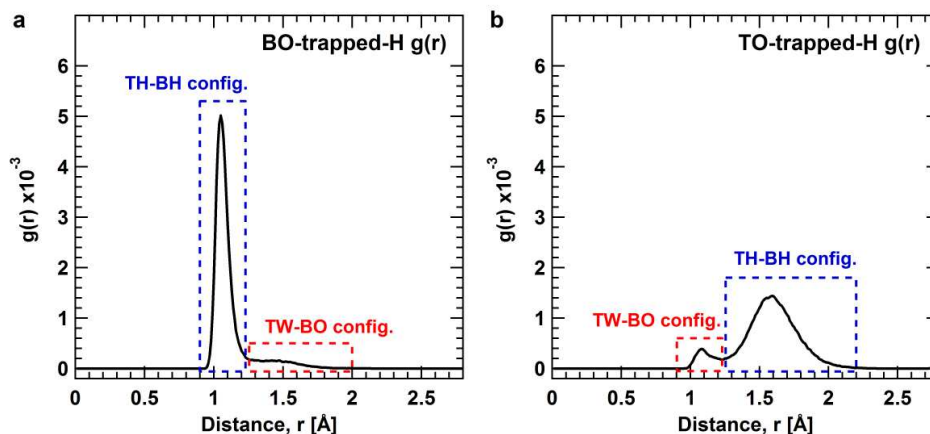


Fig. S5. The pair distribution functions, $g(r)$, of the (a) BO-trapped-H pairs, and (b) TO-trapped-H pairs in the TH-BH and TW-BO configurations. The covalent and H-bonded contributions are defined by the O-H distances as ~ 1.06 Å and 1.25-2.3 Å, respectively. The TH-BH configurations occur 90% of the time during the simulation and yield larger peaks (highlighted by blue boxes) than the TW-BO configurations. In the TH-BH configuration, the H-bond lengths of the TO-trapped-H pairs show large variations as indicated by the broad distributions in (b). This is a result of the relatively free motion of the TO atoms, which is the source of the broad 230-430 meV band shown in Fig. S3c (i.e. trapped-H moving along the line between BO and TO in the y -direction).

Spectral decomposition on the simulated *full* sample VDOS $G(E)$

To add more insights to the simulated *full* sample spectrum, the VDOS contributions from different layers of hydrogen atoms (L_1 , L_2 and L_3) were performed using a similar decomposition route as to the one applied in the *dry* sample cell. Hydrogen atoms (as hydroxyls or water molecules) in each layer were first identified based on the corresponding axial (surface-normal) density profiles of oxygen atoms as a height away from the (110) surface plane. The decomposed hydrogen VDOS was then simulated with two subgroups of hydrogen atoms (Fig. S6). The first group refers to the hydrogen atoms in the L_1 and L_2 layers which have L_1 - L_2 interlayer interactions through H-bonds, excluding those that have H-bonds primarily with nearby water

molecules in the same layer. The second group refers to the hydrogen atoms in the L_2 and L_3 layers that have L_2 - L_3 interlayer interactions through H-bonds.

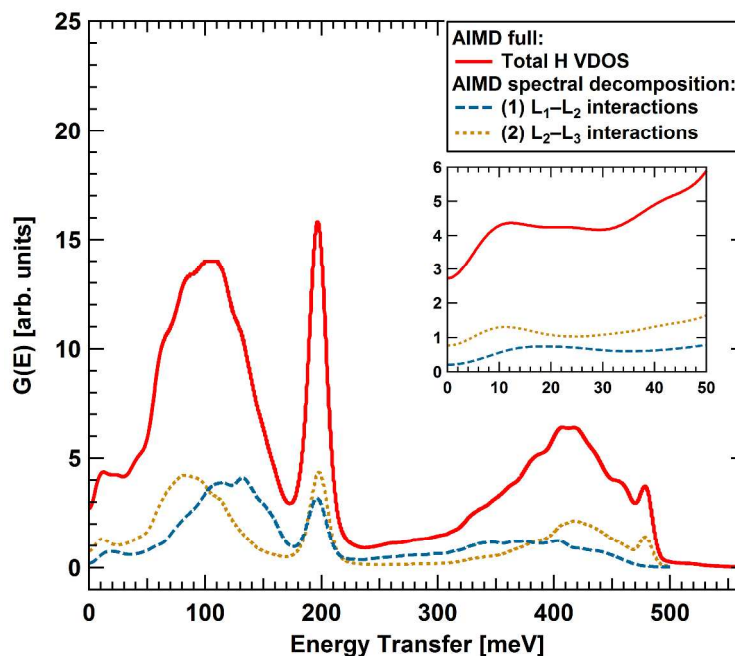


Fig. S6. Hydrogen VDOS from AIMD simulations at 300 K as a function of energy transfer for the *full* sample. Contributions to the O-H stretching band of the VDOS from L_1 - L_2 and L_2 - L_3 interlayer interactions are marked by blue and brown lines. The insert graph illustrates the contributions at the 0-50 meV energy transfer region. The sharp peak at 480 meV is mainly produced by covalent OH bonds at the interface between water and vacuum included in the L_3 .

We focused mainly on the interlayer interactions and thus not all the hydrogen atoms were considered, such as, those pointing into vacuum (in L_3) or those have H-bonds with oxygen atoms in the same layer. The sum of VDOS from these two subgroups hence does not add up to the total hydrogen VDOS. As shown in Fig. S6, the lower energy end of the O-H stretching band is dominated by the first group of hydrogen atoms, indicating stronger surface- L_1 and L_1 - L_2 interactions. The higher energy end of the O-H stretching band is, conversely, dominated by the second group of hydrogen atoms, which suggests that the L_2 - L_3 interactions are weaker due to the screening produced by the dissociation (60%) of L_1 and the fine-tuning of the hydrogen-bond strengths between L_1 and L_2 . Interestingly, the ice-like acoustic peak observed at about 8 meV and the libration-edge featured at about 62 meV are contributed mainly by the second group of hydrogen atoms (L_3 water in specific), which is entirely consistent with our arguments on the strong screening due to strong surface-H bonds in the SnO_2 system.

4. SI Text: Relation between the dissociation energy of the H-bond, its length, and the O-H stretching vibrational frequency

As with all bonds, the H-bond is characterized by its dissociation energy and the bond length. Dissociation energies (enthalpy), ΔH of H-bonds span two orders of magnitude from 0.84-167 kJ/mol (0.2-40 kcal/mol or 8.7-1731 meV/bond) (16). The bond length can be described by two distances, the distance between the hydrogen and the acceptor, d_{AH} , and the distance between the donor and the acceptor, d_{XA} . Using the H-bonds observed in water as a definition of moderate bonds, Jeffrey (17) defines strong bonds as those with $d_{AH} < 1.5 \text{ \AA}$, moderate with $1.5 \text{ \AA} < d_{AH} < 2.2 \text{ \AA}$, and weak with $2.2 \text{ \AA} < d_{AH}$.

The H-bond lowers the vibrational frequency of the donor-hydrogen stretching mode, ν_0 . This characteristic redshift, $\Delta\nu = \nu_0 - \nu$, is correlated with the dissociation energy and the bond distance. Since, the enthalpy, the distance, and the red shift, are three interrelated characteristics of the H-bond that are accessible from different experimental and theoretical methods, the study of their mutual dependence has been the focus of intense investigation and debate.

In 1937, Badger and Bauer proposed a linear relation between the redshift and the energy (18). However, the fit to experimental data shows that the relation is not necessarily true and the accumulation of data shows that the relation is non-linear. Based on the charge transfer theory of Mulliken and Person (16), Rao and coworkers (20) derived the following relation between the dissociation enthalpy and the redshift

$$H_R = \beta \sqrt{\nu_0^2 - \nu^2}. \quad (1)$$

A large compilation of experimental data (20, 21) indicates that β is about 0.016 kJ/(mol cm^{-1}).

An alternative route to derive the relation between the red shift and the bond enthalpy is based on the proportionality between bond enthalpy and the change in the square root of the integrated infrared intensity proposed by Iogansen (22). Although the square root intensity relation to the H-bond enthalpy was based on observations of H-bonds in solution, it is expected to be also valid for hydroxylated surfaces. Indeed, Kiselev found that the proportionality persists for measurements on hydroxylated silica as seen in Fig. 8 of ref. (23). Kiselev (23) ascribes the difference observed in the proportionality coefficient to the uncertainty of the determination of the hydroxylated area on surfaces as compared with solutions. Using this idea, Iogansen (24) derived the relation

$$-\Delta H_I = \partial \sqrt{\nu_0 - \nu}, \quad (2)$$

with α about 1.3 kJ/(mol cm⁻¹) based on fitting a large set of experimental data. The two relations are plotted in Fig. S7. As expected, both relations match at low H- bond strength and divert for bond energies > 30 kJ/mol.

Rozenberg, Loewenschuss, and Marcus (25) measured the stretching frequency redshift, $\Delta\nu = \nu_0 - \nu$, and the H-bond distance for a set of crystals. These authors found that the experimental data is well represented by the relation

$$\frac{\Delta\nu}{\text{cm}^{-1}} = 0.011 \left(\frac{d_{AH}}{\text{nm}} \right)^{-6.1} \quad (3)$$

This relation is compared with the frequencies collected by Libowitzky (26) and depicted in Fig. 4 (main text). *According to these theories, we estimate that the H-bond strength on the dry surface of SnO₂ is of the order of 45-50 kJ/mol, while in water this value is of the order of 25 kJ/mol for the liquid and 28 kJ/mol for ice (27).*

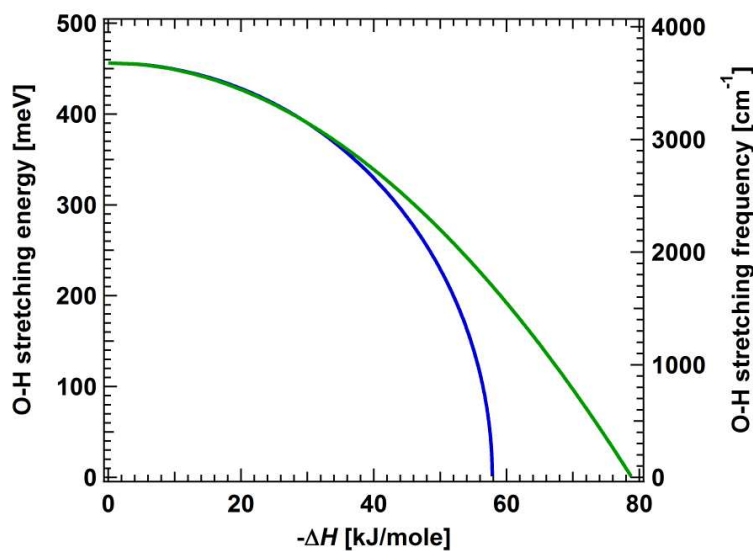


Fig. S7. O-H stretching frequency vs. H-bond strength. The blue line corresponds to the model by Rao et al. (20) (equation **Error! Reference source not found.**) and the green to the model by Iogansen (24) (equation **Error! Reference source not found.**).

Supplementary References

1. Wang H-W, et al. (2013) Structure and stability of SnO₂ nanocrystals and surface-bound water species. *J Am Chem Soc* 135(18):6885–6895.
2. Granroth GE, et al. (2010) SEQUOIA: A newly operating chopper spectrometer at the SNS. *J Phys Conf Ser* 251(1):012058.
3. Kumar N, et al. (2011) Faster proton transfer dynamics of water on SnO₂ compared to TiO₂. *J Chem Phys* 134(4):044706.
4. Bandura AV, Sofo JO, Kubicki JD (2006) Derivation of force field parameters for SnO₂-H₂O surface systems from plane-wave density functional theory calculations. *J Phys Chem B* 110(16):8386–8397.
5. Kresse G, Hafner J (1993) Ab initio molecular dynamics for liquid metals. *Phys Rev B* 47(1):558–561.
6. Kresse G, Hafner J (1994) Ab initio molecular-dynamics simulation of the liquid-metal-amorphous-semiconductor transition in germanium. *Phys Rev B* 49(20):14251–14269.
7. Kresse G, Furthmüller J (1996) Efficiency of ab-initio total energy calculations for metals and semiconductors using a plane-wave basis set. *Comput Mater Sci* 6(1):15–50.
8. Kresse G, Furthmüller J (1996) Efficient iterative schemes for ab initio total-energy calculations using a plane-wave basis set. *Phys Rev B* 54(16):11169–11186.
9. Blöchl PE (1994) Projector augmented-wave method. *Phys Rev B* 50(24):17953–17979.
10. Kresse G, Joubert D (1999) From ultrasoft pseudopotentials to the projector augmented-wave method. *Phys Rev B* 59(3):1758–1775.
11. Perdew JP, Burke K, Ernzerhof M (1996) Generalized gradient approximation made simple. *Phys Rev Lett* 77(18):3865.
12. Perdew JP, Burke K, Ernzerhof M (1997) Generalized gradient approximation made simple [Phys Rev Lett 77, 3865 (1996)]. *Phys Rev Lett* 78(7):1396–1396.
13. Kneller GR, Keiner V, Kneller M, Schiller M (1995) nMOLDYN: A program package for a neutron scattering oriented analysis of Molecular Dynamics simulations. *Comput Phys Commun* 91(1):191–214.
14. Róg T, Murzyn K, Hinsien K, Kneller GR (2003) A program package for a neutron scattering oriented analysis of molecular dynamics simulations. *J Comput Chem* 24(5):657–667.
15. nMOLDYN users's guide - Theoretical Biophysics, Molecular Simulation, and Numerically Intensive Computation. at <http://dirac.cnrs-orleans.fr/plone/software/nmoldyn/nmoldyn_user_guide.pdf/view>
16. Steiner T (2002) The hydrogen bond in the solid state. *Angew Chem Int Ed* 41(1):48–76.
17. Jeffrey GA (1997) *An Introduction to Hydrogen Bonding*. (Oxford University Press).
18. Badger RM, Bauer SH (1937) Spectroscopic studies of the hydrogen bond. ii. The shift of the O-H vibrational frequency in the formation of the hydrogen bond. *J Chem Phys* 5(11):839–851.
19. Mulliken RS, Person WB (1962) Donor-acceptor complexes. *Annu Rev Phys Chem* 13(1):107–126.
20. Rao CNR, Dwivedi PC, Ratajczak H, Orville-Thomas WJ (1975) Relation between O-H stretching frequency and hydrogen bond energy: Re-examination of the Badger-Bauer rule. *J Chem Soc, Faraday Trans 2* 71:955–966.
21. Ratajczak H, Orville-Thomas WJ, Rao CNR (1976) Charge transfer theory of hydrogen bonds: relations between vibrational spectra and energy of hydrogen bonds. *Chem Phys* 17(2):197–216.
22. Iogansen AV (1965) Relation between hydrogen bond energy and intensity of infrared absorption. *Dokl Akad Nauk Sssr* 164:610.
23. Kiselev AV (1971) The effect of the geometrical structure and the chemistry of oxide surfaces on their adsorption properties. *Discuss Faraday Soc* 52:14–32.
24. Iogansen AV (1999) Direct proportionality of the hydrogen bonding energy and the intensification of the stretching $\nu(\text{XH})$ vibration in infrared spectra. *Spectrochimica Acta A: Mol Biomol Spectrosc* 55(7):1585–1612.
25. Rozenberg M, Loewenschuss A, Marcus Y (2000) An empirical correlation between stretching vibration redshift and hydrogen bond length. *Phys Chem Chem Phys* 2(12):2699–2702.
26. Libowitzky E (1999) in *Hydrogen Bond research*, eds Schuster P, Mikenda W (Springer, Vienna), pp 103–115.
27. Suresh SJ, Naik VM (2000) Hydrogen bond thermodynamic properties of water from dielectric constant data. *J Chem Phys* 113(21):9727–9732.